A numerical study of the solution of x-mode equations around the hybrid resonance

Céline Caldini-Queiros, Bruno Després, Lise-Marie Imbert-Gérard, Maryna Kachanovska

A NUMERICAL STUDY OF THE SOLUTION OF X-MODE EQUATIONS AROUND THE HYBRID RESONANCE *

Céline Caldini-Queiros[1], Bruno Després[2], Lise-Marie Imbert-Gérard[3] and Maryna Kachanovska[4]

Abstract. Hybrid resonance is a physical phenomenon that appears for example in the heating of plasma, and as such is of scientific interest in the development of the ITER project. In this paper we focus some solutions with low regularity of Maxwell equations in plasmas under strong background magnetic field. Our main purpose is two-fold. On one hand we investigate the finite element approximation of the one dimensional problem written in the frequency domain, and on the other hand we investigate two different finite difference approximations of the one dimensional time dependent problem. We will also compare the results of these different methods.

Résumé. La résonnance hybride est un phénomène physique qui apparait par exemple lorsque l'on chauffe un plasma, et ainsi est d'intérêt scientifique dans le cadre du développement du projet ITER. Dans ce papier, nous nous concentrons sur certaines solutions faiblement régulières des équations de Maxwell pour les plasmas sous l'influence de champ magnétiques forts. Notre but principal est ici double. D'un côté nous évaluons l'approximation numérique à l'aide d'éléments finis en une dimension en formulation fréquentielle, et de l'autre nous étudions l'approximation numérique à l'aide de deux méthodes de différences finies pour la formulation temporelle monodimensionelle. Nous comparons les résultats de ces différentes méthodes.

1. Introduction

Modelling various phenomena in plasmas is of practical importance for developing new sources of energy based on plasma fusion, see the ITER project[1]. This article concentrates on studying a phenomenon of hybrid resonance [15], which is observed in experiments (see [6, 7, 9]) and is described mathematically as the non-regularity of the solutions of Maxwell equations in plasmas under strong background magnetic field [8]. The energy deposit is resonant and may exceed by far the energy exchange which occurs in Landau damping, see [10]. Contrary to the Landau damping, however, hybrid resonance appears in a simpler model coupling fluid equations with the non electrostatic part of Maxwell equations.

* The authors acknowledge the support of ANR under contract ANR-12-BS01-0006-01. Moreover, this work was carried out within the framework of the European Fusion Development Agreement and the French Research Federation for Fusion Studies. It is supported by the European Communities under the contract of Association between Euratom and CEA. The views and opinions expressed herein do not necessarily reflect those of the European Commission.

[1] Max Planck Institute für PlasmaPhysik, Garching bei München, Germany

[2] Sorbonne Universités, UPMC Univ Paris 06, UMR 7598, Laboratoire Jacques-Louis Lions, F-75005, Paris, France

[3] Courant Institute of Mathematical Sciences, New York University

[4] POEMS, INRIA, ENSTA ParisTech, Palaiseau, France

[1] www.iter.org

We consider the model of cold plasma of [15] which is described by the 2D time-dependent Maxwell system

$$\begin{aligned} -\varepsilon_0 \partial_t \mathbf{E} + \mathbf{curl}\, \mathbf{H} &= \mathbf{J} \\ \mu_0 \partial_t \mathbf{H} + \mathbf{curl}\, \mathbf{E} &= 0 \end{aligned}$$

coupled with a linear electronic current $\mathbf{J} = eN_e \mathbf{u}_e$,

$$m_e \partial_t \mathbf{u}_e = e(\mathbf{E} + \mathbf{u}_e \wedge B_0) - m_e \nu \mathbf{u}_e,$$

where ν is the friction between particles. The unknowns are the electromagnetic fields $(\mathbf{E}, \mathbf{H})$ with the usual notation $\mathbf{H} = \mathbf{B}/\mu_0$, and the velocity of electrons $\mathbf{u}_e$. Here B_0 is the background magnetic field, typically assumed to be uniform in time and space. We denote by $e < 0$ the value of the charge of electrons, m_e the electron mass and N_e the electron density that in general depends on spatial variables and is uniform in time. Without loss of generality, we set $\mathbf{B}_0 = (0,\ 0,\ B_0)$, which allows to obtain the following system of 1D equations

$$\begin{cases} \epsilon_0 \partial_t E_x = -eN_e u_x, \\ \epsilon_0 \partial_t E_y + \partial_x H_z = -eN_e u_y, \\ \mu_0 \partial_t H_z + \partial_x E_y = 0, \\ m_e \partial_t u_x = eE_x + eu_y B_0 - \nu m_e u_x, \\ m_e \partial_t u_y = eE_y - eu_x B_0 - \nu m_e u_y \end{cases} \tag{1}$$

posed in $(-L,\ \infty) \times \mathbb{R}$, for some $L > 0$. This domain represents the physical case of a wave sent from a wall facing a plasma. The energy of this system for $\nu = 0$ in a domain $\Omega \in \mathbb{R}^2$ can be expressed as [4]

$$\mathcal{E}(t) = \int_\Omega \left(\frac{\epsilon_0 |\mathbf{E}(t,\mathbf{x})|^2}{2} + \frac{|\mathbf{B}(t,\mathbf{x})|^2}{2\mu_0} + \frac{m_e |\mathbf{J}(t,\mathbf{x})|^2}{2|e|N_e(\mathbf{x})} \right) \mathrm{d}\mathbf{x}.$$

In [8] it was shown that the time harmonic electric field component E_x in this case is not necessarily square integrable, and explicit estimates on the behavior of the solutions of (1) in 1D were provided. This apparent paradox is of course the source of important numerical difficulties which are the subject of the present study.

We complement Problem (1) with the boundary conditions. At the left boundary of the domain, which represents the wall of the Tokamak, we choose Robin boundary conditions

$$-\, curl \mathbf{E} - \imath\lambda \mathbf{E} \wedge \mathbf{n} = g_{inc} = -curl \mathbf{E}_{inc} - \imath\lambda \mathbf{E}_{inc} \wedge \mathbf{n}, \tag{2}$$

where $\mathbf{E}_{inc} = \exp(\imath\lambda x) \begin{pmatrix} E_1 \\ E_2 \end{pmatrix}$ and λ is the frequency of the antenna. We truncate the domain $(-L,\ \infty)$ to $(-L,\ H)$ and set on the right boundary $\mathrm{curl}\, \mathbf{E} = 0$.

The goal of this article is three-fold. First, we investigate the finite element approximation of the 1D problem (1) written in the frequency domain ($\partial_t \to -i\omega$), with a linearized dielectric tensor with respect to ν. In particular, we again investigate this problem in one dimension, performing the Fourier transform in y. We prove the well-posedness of this problem for $\nu > 0$ in Section 2.1 and demonstrate that the use of (P1) finite elements allows to approximate the singularity of the solution fairly well (Section 4.1). Second, we briefly develop an original scheme based on widely appreciated semi-lagrangian schemes for the discretization of time domain Maxwell's equations with a linear current. Thirdly, we consider the case $\nu \to 0$, and study the limiting amplitude solution $\lim_{t\to+\infty} \lim_{\nu\to 0} \mathbf{E}(t)$ obtained with the help of the FDTD discretization of (1), suggested in [4]. We compare this result with $\hat{\mathbf{E}} \mathrm{e}^{i\omega t}$, computed in the frequency domain, for $\nu \to 0$, which is equivalent to considering $\lim_{\nu\to 0} \lim_{t\to+\infty} \mathbf{E}(t)$. Such a comparison is a way to study the formal commutation relation

$$\lim_{\nu\to 0} \lim_{t\to+\infty} = \lim_{t\to+\infty} \lim_{\nu\to 0},$$

$$\begin{array}{ccc} \mathbf{E}^{\nu}(t) & \xrightarrow{\quad \nu \to 0+ \quad} & \mathbf{E}^{0+}(t) \\ \Big\downarrow {\scriptstyle t \to +\infty} & & \Big\downarrow {\scriptstyle t \to +\infty} \\ \hat{\mathbf{E}}^{\nu}(t)\mathrm{e}^{i\omega t} & \xrightarrow{\quad \nu \to 0 \quad} & \lim\limits_{\nu\to 0}\lim\limits_{t\to\infty} \mathbf{E}^{\nu}(t) = \lim\limits_{t\to\infty}\lim\limits_{\nu\to 0} \mathbf{E}^{\nu}(t) \end{array}$$

FIGURE 1. Schematic representation of the equivalence of the limited absorption and limiting amplitude principles.

see Figure 1. Even though it is true for standard linear wave problems, it is not clear that it still hold in our case due the singularity of the hybrid resonance.

To our knowledge, such numerical studies have not been performed in the existing literature.

2. Frequency domain study

In the frequency domain, the velocity can be eliminated and it yields a simpler system under the form of Maxwell equations with the cold plasma dielectric tensor [8, 15]. One obtains the equations

$$\begin{aligned} \operatorname{curl}\operatorname{curl}\hat{\mathbf{E}} - \epsilon(\omega)\hat{\mathbf{E}} = 0, \\ \epsilon(\omega) = \begin{pmatrix} \tilde{\alpha} & i\tilde{\delta} \\ -i\tilde{\delta} & \tilde{\alpha} \end{pmatrix}, \\ \tilde{\alpha}(\omega) = \frac{\omega^2}{c^2}\left(1 - \frac{\tilde{\omega}\omega_p^2}{\omega(\tilde{\omega}^2 - \omega_c^2)}\right), \qquad \tilde{\delta}(\omega) = \frac{\omega_c\omega_p^2}{\omega(\tilde{\omega}^2 - \omega_c^2)}, \end{aligned}$$

where the frequency $\tilde{\omega} = \omega + i\nu$ is shifted in the complex plane, the cyclotron frequency is $\omega_c = \frac{eB_0}{m_e}$ and the plasma frequency is $\omega_p^2 = \frac{e^2 N_e}{\epsilon_0 m_e}$. The series expansion as $\nu \to 0$ gives at leading orders

$$\begin{aligned} \tilde{\alpha}(\omega) = \alpha(\omega) + i\nu\frac{\omega_p^2(\omega^2+\omega_c^2)}{(\omega^2-\omega_c^2)^2}\frac{\omega^2}{c^2}, \qquad \alpha(\omega) = \frac{\omega^2}{c^2}\left(1 - \frac{\omega_p^2}{\omega^2-\omega_c^2}\right), \\ \tilde{\delta}(\omega) = \delta(\omega) - \frac{2i\omega^3\nu}{c^2(\omega^2-\omega_c^2)^2}, \qquad \delta(\omega) = \frac{\omega\omega_c\omega_p^2}{c^2(\omega^2-\omega_c^2)}. \end{aligned}$$

We finally obtain a simpler equation [8]

$$\operatorname{curl}\operatorname{curl}\hat{\mathbf{E}} - \frac{\omega^2}{c^2}\left(\epsilon_0(\omega) + \nu Id\right)\hat{\mathbf{E}} = 0, \tag{3}$$

$$\epsilon_0(\omega) = \begin{pmatrix} \alpha & i\delta \\ -i\delta & \alpha \end{pmatrix}. \tag{4}$$

In this model problem, the coefficients $\alpha(\omega)$ and $\delta(\omega)$ are sufficiently smooth, i.e. bounded and continuous in $[-L,\ \mathbb{R})$.

2.1. 1D case

In order to reduce problem (3) to one dimension, perform a Fourier transform in the y variable, denoting by θ the corresponding Fourier variable. After introducing $\Omega = (-L,\ H) \subset \mathbb{R}$ and defining the function space of

the problem $\mathbf{V} = L_2(\Omega) \times H_1(\Omega)$, equipped with the norm

$$\|\mathbf{v}\|_{\mathbf{V}}^2 = \|v_1\|_{L_2(\Omega)}^2 + \|v_2\|_{H^1(\Omega)}^2,$$

the resulting one-dimensional system can be rewritten in the following variational form:

$$\int_{-L}^{H} (E_y' - \imath\theta E_x)\overline{(\tilde{E}_y' - \imath\theta\tilde{E}_x)} - \int_{-L}^{H} (\varepsilon_0 + \imath\nu Id)\mathbf{E}\cdot\overline{\tilde{\mathbf{E}}} - \imath\lambda E_y(-L)\overline{\tilde{E}_y(-L)} = -g_{inc}(-L)\overline{(\tilde{E}_y(-L))}, \qquad (5)$$

$$\text{for all } \tilde{\mathbf{E}} = (\tilde{E}_x, \tilde{E}_y) \in \mathbf{V}.$$

Recall that here $\lambda \geq 0$. Let us remark that in this and further sections, where it is not ambiguous, we will use the notation $E_{x,y}$ instead of $\hat{E}_{x,y}$ for convenience.

The above can be reformulated as

$$a(\mathbf{u}, \mathbf{v}) = l(\mathbf{v}), \quad \text{for all } \mathbf{v} \in \mathbf{V}, \qquad (6)$$

with a bilinear form a and a linear form l:

$$a(\mathbf{u}, \mathbf{v}) = a_1(\mathbf{u}, \mathbf{v}) + \imath a_2(\mathbf{u}, \mathbf{v}) \quad \text{and} \quad l(\mathbf{v}) = -g_{inc}(-L)\overline{(v_2(-L))} \qquad (7)$$

where $a_1 = a_1^*$ and $a_2 = a_2^*$ are hermitian

$$\begin{cases} a_1(\mathbf{u}, \mathbf{v}) = \int_{-L}^{H} (u_2' - \imath\theta u_1)\overline{(v_2' - \imath\theta v_1)} - \int_{-L}^{H} \varepsilon_0 \mathbf{u}\cdot\overline{\mathbf{v}}, \\ a_2(\mathbf{u}, \mathbf{v}) = -\nu \int_{-L}^{H} \mathbf{u}\cdot\overline{\mathbf{v}} - \lambda u_2(-L)\overline{v_2(-L)}, \end{cases} \qquad (8)$$

The unknown is $\mathbf{u} = (E_x, E_y) = (u_1, u_2)$ and $\mathbf{v}$ is a test function.

Let us denote the spectral radius of ε_0 by $\hat{\varepsilon} = \|\rho(\varepsilon_0)\|_{L^\infty}$.

We now prove the following result.

Lemma 2.1. *If $\hat{\varepsilon} < +\infty$, the bilinear form*

$$a(\mathbf{u}, \mathbf{v}) : \mathbf{V} \times \mathbf{V} \to \mathbb{C}$$

is continuous and coercive for all $\nu \neq 0$: for all $\mathbf{u}, \mathbf{v} \in \mathbf{V}$ it holds that

$$\begin{cases} \Re\left(\mathrm{e}^{i\alpha_\nu} a(\mathbf{u}, \mathbf{u})\right) \geq \frac{|\nu|}{\sqrt{(\hat{\varepsilon}+\theta^2+1)^2+\nu^2}} \left(\frac{1}{2}\|u_2'\|_{L^2}^2 + \|\mathbf{u}\|_{L^2}^2\right), \quad \text{for some } \alpha_\nu \in \left(-\frac{\pi}{2}, 0\right) \cup \left(0, \frac{\pi}{2}\right), \\ |a(\mathbf{u}, \mathbf{v})| \leq C\|\mathbf{u}\|_{\mathbf{V}}\|\mathbf{v}\|_{\mathbf{V}}, \end{cases}$$

where $C > 0$ does not depend on ν. The problem (5) is well-posed in $\mathbf{V}$.

Proof. The boundedness of a is obvious using the continuous embedding in dimension one $H_1(\Omega) \subset C^0(\overline{\Omega})$. Let us focus on the proof of coercivity. Without loss of generality let us assume that $\nu > 0$. We denote $\hat{\varepsilon} = \|\rho(\varepsilon_0)\|_{L^\infty}$, the spectral radius of ε_0 so that $\hat{\varepsilon}Id - \varepsilon_0$ is a non negative hermitian matrix. Therefore

$$a_1(\mathbf{u}, \mathbf{u}) + \hat{\varepsilon}\|\mathbf{u}\|_{L^2}^2 = \|u_2' - \imath\theta u_1\|_{L^2}^2 + ((\hat{\varepsilon}Id - \varepsilon_0)\mathbf{u}, \overline{\mathbf{u}}) \geq \|u_2' - \imath\theta u_1\|_{L^2}^2 \geq \frac{1}{2}\|u_2'\|_{L^2}^2 - \theta^2\|u_1\|_{L^2}^2. \qquad (9)$$

Thus one can write $a_1(\mathbf{u}, \mathbf{u}) \geq \frac{1}{2}\|u_2'\|_{L^2}^2 - (\hat{\varepsilon} + \theta^2)\|\mathbf{u}\|_{L^2}^2$. One also has that $a_2(\mathbf{u}, \mathbf{u}) \leq -\nu\|\mathbf{u}\|_{L^2}^2$. Therefore

$$a_1(\mathbf{u}, \mathbf{u}) - \frac{\hat{\varepsilon} + \theta^2 + 1}{\nu} a_2(\mathbf{u}, \mathbf{u}) \geq \frac{1}{2}\|u_2'\|_{L^2}^2 + \|\mathbf{u}\|_{L^2}^2,$$

or, introducing $\alpha_\nu = \arccos \frac{1}{\sqrt{1+(\hat{\varepsilon}+\theta^2+1)^2\nu^{-2}}}$, this is equivalent to

$$\Re\left(\mathrm{e}^{i\alpha_\nu} a(\mathbf{u},\mathbf{u})\right) \geq \frac{1}{\sqrt{1+\left(\hat{\varepsilon}+\theta^2+1\right)^2\nu^{-2}}}\left(\frac{1}{2}\|u_2'\|_{L^2}^2+\|\mathbf{u}\|_{L^2}^2\right) \geq \frac{\nu}{\sqrt{(\hat{\varepsilon}+\theta^2+1)^2+\nu^2}}\left(\frac{1}{2}\|u_2'\|_{L^2}^2+\|\mathbf{u}\|_{L^2}^2\right).$$

The problem (5) is uniquely solvable thanks to Lax-Milgram theorem. □

Remark 2.2. *The above proof is not optimal in the case when $|\alpha(x)| > c > 0$ for $c > 0$ on the whole interval $[-L,\ H]$, at least for the case $\theta = 0$. In this case the problem (10) is well-posed for $\nu = 0$. More precisely, it can be written as a system of two equations, where the first equation (for E_y) is the variational formulation for the Helmholtz equation with the variable coefficient $k^2 = (\alpha - \frac{\delta^2}{\alpha})$, and the second equation*

$$(E_x, u) = -\left(\frac{i\delta}{\alpha}E_y, u\right), \quad \textit{for all } u \in L_2(\Omega),$$

uniquely defines $E_x \in L_2(\Omega)$. The well-posedness of the former problem, with additional assumptions on boundary conditions and smoothness of the coefficients, was demonstrated in [12]. Provided the solution $E_y \in H_1(\Omega)$, we can obtain E_x from the second equation.

2.2. **Discretization of the Frequency Domain Problem**

Testing the variational formulation (5) with $(\tilde{E}_x, 0)$ and $(0,\ \tilde{E}_y) \in \mathbf{V}(\Omega)$ and using an explicit expression for the tensor of the dielectric permittivity (4), we can rewrite it as a system of two equations

$$\begin{gathered} i\theta\int_{-L}^{H}(E_y'-\imath\theta E_x)\overline{\tilde{E}_x} - \int_{-L}^{H}\left((\alpha+i\nu)E_x+\imath\delta E_y\right)_1\overline{\tilde{E}}_x = 0, \\ \int_{-L}^{H}(E_y'-\imath\theta E_x)\tilde{E}_y' - \int_{-L}^{H}\left(-\imath\delta E_x+(\alpha+i\nu)E_y\right)_2\overline{\tilde{E}}_y - \imath\lambda E_y(-L)\tilde{E}_y(-L) = -g_{inc}(-L)\overline{(\tilde{E}_y(-L))}, \\ \text{for all } \tilde{E}_x \in L_2(\Omega),\ \tilde{E}_y \in H_1(\Omega). \end{gathered} \tag{10}$$

Let us introduce two basis function spaces $V_{E_x} = \{\psi_j\}_{j=1}^{N_1}$ and $V_{E_y} = \{\phi_i\}_{i=1}^{N_2}$. We discretize problem (10) as:

$$E_x = \sum_{k=1}^{N_1} e_{xk}\psi_k, \qquad E_y = \sum_{k=1}^{N_2} e_{yk}\phi_k.$$

Introducing the notation

$$\left(K^{\psi,\phi'}\right)_{mk} = \int_{-L}^{H}\bar{\psi}_m\phi_k'dx, \qquad \left(M^{\psi}\right)_{mk} = \int_{-L}^{H}\psi_k\bar{\psi}_m dx, \qquad \left(M^{\alpha,\psi}\right)_{mk} = \int_{-L}^{H}(\alpha(x)+i\nu)\psi_m\bar{\psi}_k dx,$$

$$\left(M^{\delta,\psi,\phi}\right)_{mk} = \int_{-L}^{H}\delta(x)\bar{\psi}_m\phi_k dx, \qquad K_{\ell k} = \int_{-L}^{H}\phi_k'(x)\bar{\phi}_\ell'(x)dx, \qquad \left(M^{\alpha,\phi}\right)_{\ell k} = \int_{-L}^{H}(\alpha(x)+i\nu)\bar{\phi}_\ell\phi_k dx,$$

$$I^{\Gamma}_{km} = \bar{\phi}_m(-L)\phi_k(-L),$$

$$\boldsymbol{e}_x = (e_{11},\ldots,e_{1N_1})^T,\ \boldsymbol{e}_y = (e_{21},\ldots,e_{2N_1})^T,$$

$\mathbf{0}_n$ is an n-dimensional zero column vector,

we rewrite the system (10) in an antisymmetric block form:

$$\begin{pmatrix} \theta^2 M^{\psi} - M^{\alpha,\psi} & i\theta K^{\psi,\phi'} - iM^{\delta,\psi,\phi} \\ -i\theta (K^{\psi,\phi'})^* + i(M^{\delta,\psi,\phi})^* & K - M^{\alpha,\phi} - i\lambda I^{\Gamma} \end{pmatrix} \begin{pmatrix} \boldsymbol{e}_x \\ \boldsymbol{e}_y \end{pmatrix} = -g_{inc}(-L) \begin{pmatrix} \mathbf{0}_{N_1} \\ \bar{\phi}_1(-L) \\ \bar{\phi}_2(-L) \\ \vdots \\ \bar{\phi}_{N_2}(-L) \end{pmatrix}.$$

This expression greatly simplifies when choosing $V_{E_x} = V_{E_y} = (\phi_m)_{m=1}^{N_2}$ and in the case $\theta = 0$. One obtains the matricial structure

$$\begin{pmatrix} M^{\alpha,\phi} & iM^{\delta,\phi,\phi} \\ i(M^{\delta,\phi,\phi})^* & K - M^{\alpha,\phi} - i\lambda I^{\Gamma} \end{pmatrix} \begin{pmatrix} \boldsymbol{e}_x \\ \boldsymbol{e}_y \end{pmatrix} = -g_{inc}(-L) \begin{pmatrix} \mathbf{0}_{N_1} \\ \bar{\phi}_x(-L) \\ \bar{\phi}_y(-L) \\ \vdots \\ \bar{\phi}_{N_2}(-L) \end{pmatrix}. \tag{11}$$

In this work we use the above formulation with the Lagrange P_1 basis elements.

3. Time Dependent Problem Discretization

Let us consider the system (1) in dimension one in the X-mode configuration which is transverse electric.

3.1. **A staggered scheme**

In this section, we develop a discretization of the time dependant problem (1) in one dimension. We compute a numerical approximation of (1) on a cartesian grid using the Yee scheme, as suggested in [4]. Let n denote the time step index, as usual $t_n = n\Delta t$. It is standard (see [4,16]) to discretize the electrical field on the integer time steps, whereas the field H_z on half time steps, $t_{n+1/2}$. The time discretization of the system reads:

$$\begin{cases} \epsilon_0 \frac{E_x^{n+1} - E_x^n}{\Delta t} = -eN_e u_x, \\ \epsilon_0 \frac{E_y^{n+1} - E_y^n}{\Delta t} + \partial_x H_z = -eN_e u_y, \\ \mu_0 \frac{H_z^{n+1/2} - H_z^{n-1/2}}{\Delta t} + \partial_x E_y - \partial_y E_x = 0, \\ m_e \frac{u_x^{n+1} - u_x^n}{\Delta t} = eE_x + eu_y B_0 - \nu m_e u_x, \\ m_e \frac{u_y^{n+1} - u_y^n}{\Delta t} = eE_y - eu_x B_0 - \nu m_e u_y. \end{cases}$$

In Yee scheme, the differents components of the vector fields are defined on staggered points. We summarize this discretization on Fig. 2 where the positions of Ex, u_x (black dots), E_y, u_y (blue dots) and H_z (red dots) on the discretized grid in space and time are shown. The fully discretized system then reads

$$\begin{aligned} \varepsilon_0 \frac{E_x\,|_i^{n+1} - E_x\,|_i^n}{\Delta t} &= -eN_e \frac{u_x\,|_i^{n+1} + u_x\,|_i^n}{2}, \\ \varepsilon_0 \frac{E_y\,|_{i+1/2}^{n+1} - E_y\,|_{i+1/2}^n}{\Delta t} + \frac{H_z\,|_{i+1}^{n+1/2} - H_z\,|_i^{n+1/2}}{\Delta x} &= -eN_x \frac{u_y\,|_{i+1/2}^{n+1} + u_y\,|_{i+1/2}^n}{2}, \\ \frac{H_z\,|_i^{n+1/2} - H_z\,|_i^{n-1/2}}{\Delta t} + \frac{E_y\,|_{i+1/2}^n - E_y\,|_{i-1/2}^n}{\Delta x} &= 0, \\ m_e \frac{u_x\,|_i^{n+1} - u_x\,|_i^n}{\Delta x} = eN_e \frac{E_x\,|_i^{n+1} + E_x\,|_i^n}{2} - \nu m_e \frac{u_x\,|_i^{n+1} + u_x\,|_i^n}{2} &+ eB_0 \frac{u_y\,|_{i+1/2}^n + u_y\,|_{i+1/2}^{n+1}}{2}, \end{aligned}$$

$$m_e \frac{u_y\,|_{i+1/2}^{n+1} - u_y\,|_{i+1/2}^{n}}{\Delta t} = eN_e \frac{E_y\,|_{i+1/2}^{n+1} + E_y\,|_{i+1/2}^{n}}{2} - \nu m_e \frac{u_y\,|_{i+1/2}^{n+1} + u_y\,|_{i+1/2}^{n}}{2} - eB_0 \frac{u_x\,|_{i}^{n} + u_x\,|_{i}^{n+1}}{2},$$

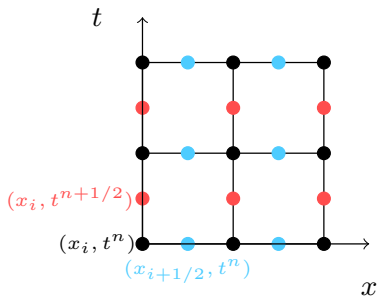

FIGURE 2. Positions of E_x, u_x (black dots), E_y, u_y (blue dots) and H_z (red dots) on the discretized grid in space and time

It is possible to rewrite this system in an explicit form (we omit here these simple but slightly tedious computations).

3.2. **A co-localized scheme based on semi-lagrangian discretisation**

The scheme that is described hereafter is mentioned since it is based on some well-known numerical methods in plasma physics, the so-called semi-lagrangian schemes which are widely used for the numerical approximation of transport equations. It seems to be an original use of semi-lagrangian schemes and is mentioned since it can be an option. We restrict the presentation to the minimum and leave the details of the construction to the alert reader.

The idea is to split the system (1) into a series of transport equations (here just 2) and a local in-the-cell system.

- At time step $t_n = n\Delta t$, all quantities are given $(E_x, E_y, H_z, u_x, u_y)_i^n$ in the cells, that is for all i in the computational domain.
- The first step is to solve

$$\begin{cases} \epsilon_0 \partial_t E_x = 0, \\ \epsilon_0 \partial_t E_y + \partial_x H_z = 0, \\ \mu_0 \partial_t H_z + \partial_x E_y = 0, \\ m_e \partial_t u_x = 0, \\ m_e \partial_t u_y = 0. \end{cases}$$

Since $\epsilon_0 \mu_0 c^2 = 1$, this can be performed solving two transport equations

$$\begin{cases} \partial_t w + c\partial_x w = 0, & w = E_y + cH_z, \\ \partial_t z - c\partial_x z = 0 & z = E_y - cH_z. \end{cases}$$

In our case we used a semi-lagrangian scheme for a time step Δt. In the tests, we used Strang's stencils described in [3] with CFL $\nu = 0.5$, at order 7. It yields the chain $(E_y, H_z)_i^n \mapsto (w, z)_i^n \mapsto (w, z)_i^{n*} \mapsto (E_y, H_z)_i^{n*}$. Here $n*$ denotes the intermediate stage of the algorithm.

- The second (and final) step is to solve

$$\begin{cases} \epsilon_0 \partial_t E_x = -eN_e u_x, \\ \epsilon_0 \partial_t E_y = -eN_e u_y, \\ \mu_0 \partial_t H_z = 0, \\ m_e \partial_t u_x = eE_x + eu_y B_0 - \nu m_e u_x, \\ m_e \partial_t u_y = eE_y - eu_x B_0 - \nu m_e u_y. \end{cases}$$

This is performed locally in every cell starting from the data at the preceding step. In our case we just adapt the algorithm developed for the staggered scheme. We make sure that the method is conservative in total energy if $\nu = 0$, using a half-step discretization of the right hand sides.

- Therefore all quantities are now given $(E_x, E_y, H_z, u_x, u_y)_i^{n+1}$ in the cells at time step $t_{n+1} = (n+1)\Delta t$, and it is enough to loop in time.

Remark 3.1. *The structure of this algorithm is very similar to the one developed in [5] and can be adapted and studied numerically in any dimension on a Cartesian grid and for more complex right hand sides.*

4. Numerical Experiments

This section is organized as follows. The first part is dedicated to the numerical implementation of the frequency domain formulation (3). We study the convergence of this formulation and the behaviour of the numerical solution as the absorption parameter ν tends to zero. The experiments in this section were performed with the help of the code written in Octave. We implemented the scheme described in Section 2.2 for a case of P_1-space used for the approximation of E_x and E_y and $\theta = 0$, thus working with the system (11). We apply permutation to the above system to obtain a 7-diagonal Hermitian matrix and solve the system with the Gauss back substitution algorithm.

The intermediate part briefly validates the semi-lagrangian discretization of the time domain formulation.

The last part of the section deals with the question of the equivalence of the limiting absorption and limited amplitude principle. We compare the solutions obtained as $\nu \to 0$ with the help of our frequency domain code and of the time domain code (computed for large values of time). The time-domain code implements the scheme described in Section 2.2 and is written in Fortran.

4.1. **Frequency Domain Problem**

4.1.1. *Validity of the Implementation*

To check the validity of the code, we first perform a numerical experiment with (formally chosen) parameters:

$$\alpha(x) = x^2 + 1, \qquad \delta(x) = \left(\alpha^2 + x\alpha\right)^{\frac{1}{2}}. \tag{12}$$

Additionally, the boundary conditions read as

$$\partial_1 E_y(-L) + 2iE_y(-L) = 2iAi(-L) + Ai'(-L), \qquad \partial_1 E_y(H) = 0, \tag{13}$$

where $Ai(x)$ is the Airy function. For more detail on Airy functions and the Airy equation see [1, Chapter 10.4]. It can be shown that E_y that solves (3) in 1D, with the Fourier variable $\theta = 0$ (see (5), and $\nu = 0$, satisfies the Airy equation, and hence, with the choice of the boundary conditions as above, we obtain that $E_y = Ai(x)$ and $E_x = -i\frac{\delta(x)}{\alpha(x)}Ai(x)$ is the solution to the problem with parameters (12) and the boundary condition (13). The well-posedness of the respective variational formulation for $\nu = 0$ is due to Remark 2.2.

In Fig. 3 we demonstrate the convergence rates for this problem, comparing the solution with the known analytic solution. Importantly, the obtained convergence rates are in agreement with known estimates of the standard theory of convergence [2].

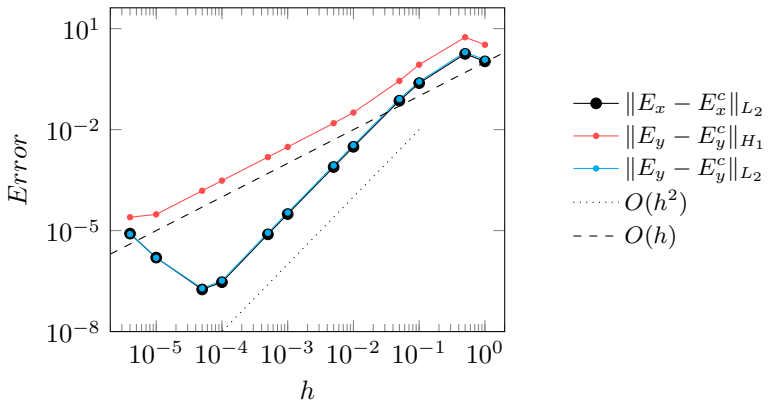

FIGURE 3. Convergence rates for the problem with parameters (12) with the boundary condition (22).

4.1.2. *Solution of X-Mode Problem*

Let us consider the case of the resonance, more precisely, we choose sufficiently smooth α, δ, s.t. $\alpha(0) = 0$ and $\delta(0) \neq 0$, and the solvability conditions of Lemma 2.1 are satisfied. For simplicity, let us assume

$$\alpha(x) = -x \text{ in some neighbourhood of } 0\ . \tag{14}$$

Given $\mathbf{V}_h = P_h^1 \times P_h^1$, with P_h^1 consisting of piecewise-linear (hat) functions, we look for a ratio $h(\nu)$ that would ensure the bound on the absolute error

$$\|E_x^\nu - E_x^{\nu,h}\|_{L_2(\Omega)} < \epsilon, \tag{15}$$

given a fixed value of $\epsilon > 0$ and $\nu \to 0$. W.l.o.g. here we assume that $\nu > 0$.

We use the following ingredients:

- The Céa's lemma applied to the problem (5); here C_c is the continuity and C_i is the coercivity constants:

$$\|\mathbf{E}^\nu - \mathbf{E}^{h,\nu}\|_V \leq \frac{C_c}{C_i} \min_{\mathbf{v}\in V_h} \|\mathbf{E} - \mathbf{v}\|_V \leq C\nu^{-1} \min_{\mathbf{v}\in V_h} \|\mathbf{E} - \mathbf{v}\|_V,\ C > 0. \tag{16}$$

  The last inequality follows from Lemma 2.1 and is valid for $\nu \to 0$.
- The form of the exact solution to the problem (5), see [8],

$$E_x^\nu = -iE_y^\nu \frac{\delta}{\alpha + i\nu} = \frac{f^\nu(x)}{\alpha(x) + i\nu}, \text{ for some } f^\nu(x) \in L_2(\Omega). \tag{17}$$

  We additionally assume that $E_y^\nu(x)$ is sufficiently smooth and $\|(E_y^\nu)''\|_{H_2(\Omega)}$ can be bounded independently of ν.
- The estimate from [2, Chapter 0] on the rate of convergence of the interpolation

$$\begin{aligned} \|v - I^h v\|_{L_2(\Omega)} &\leq Ch^2 \left|v''\right|_{L_2(\Omega)},\ C > 0, \\ \|v - I^h v\|_{H_1(\Omega)} &\leq Ch|v''|_{L_2(\Omega)},\ C > 0, \end{aligned} \tag{18}$$

  where $I^h v$ is an interpolation operator onto P_h^1.

The estimate (16) combined with (18) results in, for some $C > 0$,

$$\|E_x^\nu - E_x^{\nu,h}\|_{L_2(\Omega)} \le C\nu^{-1}h + C\nu^{-1}h^2 \| \left(E_x^\nu\right)'' \|_{L_2}, \tag{19}$$

where we used an assumption that the L_2-norm of $\left(E_y^\nu(x)\right)''$ can be bounded independently of ν.

For $E_x^\nu,\ f^\nu(x)$ in (17) being sufficiently smooth,

$$\frac{d^2}{dx^2}E_x^\nu = \frac{(f^\nu)''}{\alpha + i\nu} - 2\frac{(f^\nu)'\alpha'}{(\alpha+i\nu)^2} + \frac{f^\nu\alpha''}{(\alpha+i\nu)^3},$$

from which, together with (14), it follows that there exists $c > 0$ s.t. for all sufficiently small ν

$$\left|\frac{d^2}{dx^2}E_x^\nu\right|_{L_2}^2 \le c\int\limits_\Omega \frac{1}{(x^2+\nu^2)^3}dx \le C\nu^{-5},$$

where $C > 0$ does not depend on ν. After inserting this into (19) we obtain

$$\|E_x^\nu - E_x^{\nu,h}\|_{L_2(\Omega)} \le C\nu^{-\frac{7}{2}}h^2 + C\nu^{-1}h.$$

From this it thus follows that to ensure (15) h should be chosen as

$$h = \alpha_\epsilon \nu^{\frac{7}{4}}, \tag{20}$$

where $\alpha_\epsilon > 0$ depends on ϵ but does not depend on ν. This prediction is very severe and is due to the singular nature of the problem under consideration.

Let us check numerically whether this holds true. To do so, we conduct the numerical experiment with parameters for the problem as given in Table 1. Denoting by E_x^h the solution $E_x(x)$ computed on the mesh

Parameter	Value
$\alpha(x)$	$\begin{cases} 10, & x \le -10, \\ -x, & -10 < x \le 5, \\ -5, & x > 5. \end{cases}$
$\delta(x)$	$\begin{cases} 0, & x \le -10, \\ 4/30x + 4/3, & -10 < x \le 5, \\ 2, & x > 5. \end{cases}$
$g^{inc}(-L)$	$-2\sqrt{2}i\exp(-22\sqrt{2}i)$
λ	$\sqrt{10}$
L	15
H	10

TABLE 1. The parameters for the problem with the resonance.

with a width h, and by E_x^c the solution computed on a mesh multiple times finer, let

$$h_\epsilon = \sup\{h : \|E_x^{h'} - E_x^c\| < \epsilon \text{ for all } h' < h\}. \tag{21}$$

The computed dependence of h_ϵ on ν is shown in Fig. 4. We can see that the estimate (20) is pessimistic compared to the one suggested by (21), at least for given values of ϵ and for a chosen range of $\nu > 0$.

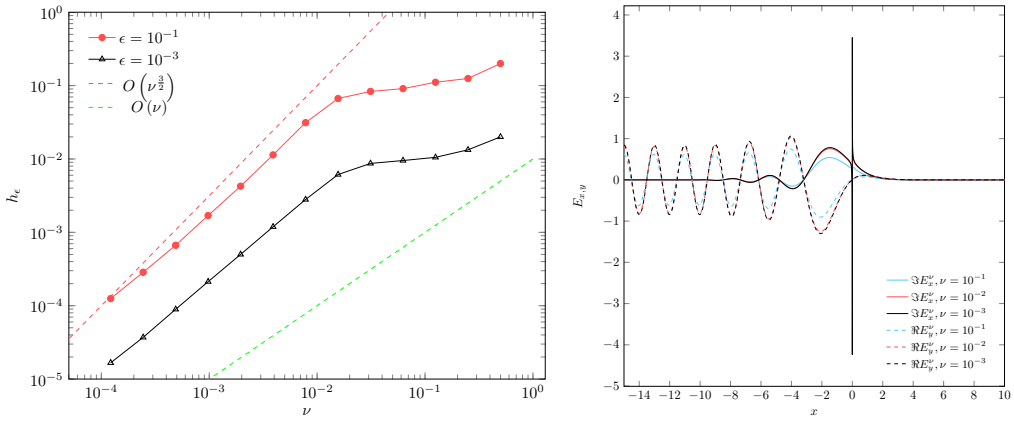

FIGURE 4. In the left figure the depenence of h_ϵ as defined by (21) on ν is demonstrated. In the right figure we show the computed solutions for the problem with parameters in Table 1 for different values of ν.

Remark 4.1. *It can be shown that* $\|E_x^\nu\|_{L_2(\Omega)} \leq \frac{C}{\sqrt{\nu}}$, $C > 0$, *and thus the relative error control*

$$\frac{\|E_x^\nu - E_x^{\nu,h}\|_{L_2(\Omega)}}{\|E_x^\nu\|_{L_2(\Omega)}} \leq \epsilon$$

is ensured by choosing h *as* $\beta_\epsilon \nu^{\frac{3}{4}}$.

In Figure 5 we demonstrate the dependence of the condition number of the matrix of the system (11) on ν, for several values of h. Remarkably, for $\nu = 0$ the computed matrices are not singular. We do not know the exact reason for this. As an additional illustration, we compare the solutions for very small ν and $\nu = 0$ for different meshes in Fig. 5.

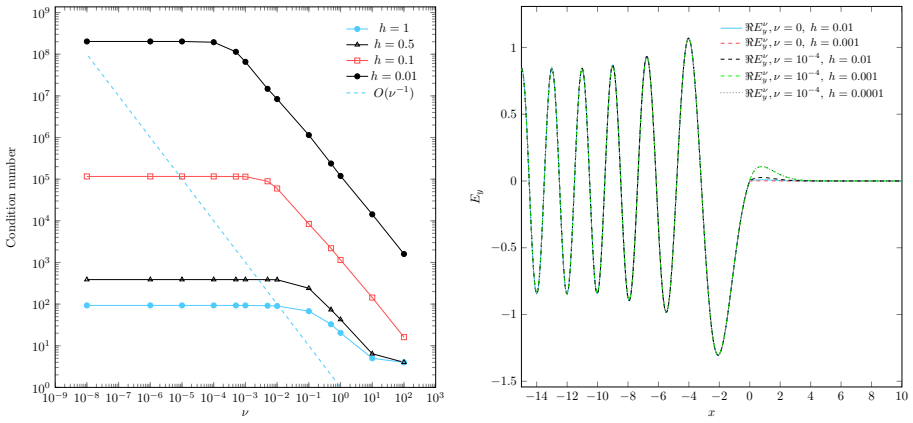

FIGURE 5. The left plot demonstrates the dependence of the condition number of the system (11) on ν, for different values of h (the condition number for $\nu = 0$ is not shown, however, for all values of h as shown in the plot, the matrix was non-singular even for $\nu = 0$). The right plot shows E_y^ν computed on different meshes for small ν. It can be seen that for $h = 10^{-2}$ and $h = 10^{-3}$ the solutions computed for $\nu = 0$ are almost indistinguishable.

h

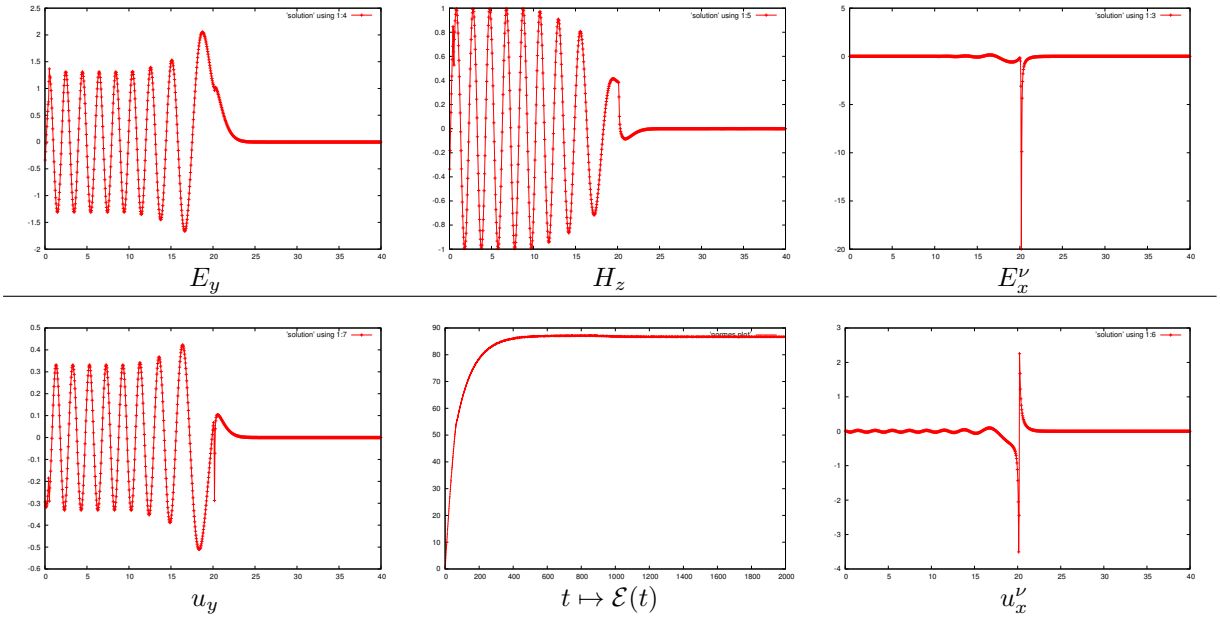

FIGURE 6. An antenna sends a time harmonic wave on the left. The medium is propagative on the left and non propagative on the right. The resonance is visible on E_x and u_x. The time of the simulation is $T = 2000$. The number of cells is typically 10000 to reach convergence.

4.2. **A validation of the semi-lagrangian scheme**

We show the results of very basic simulations that the numerical strategy based on co-localised semi-lagrangian discretization is valid even for the resonant case. The numerical tests have been kept to a minimum since much more are needed to fully validate the concept.

The setting of the numerical results of figure 6 is the following. We use a 7th order semi-lagrangian scheme, and the CFL is $\nu = 0.5$. The Pike is the hybrid resonance, visible on E_x and u_x. The total energy $\mathcal{E}(t)$ is the physical energy. The comparison with figures 4 and 9 show that the singular nature of the resonant is captured by this new scheme without any doubt.

4.3. **Limiting Amplitude and Limiting Absorption Principle**

In this section we perform several numerical experiments to check wether the limit amplitude principle and the limit absorption principle are equivalent for our problem. That is we compare the solution of the time harmonic code with the solution of the time domain staggered code.

We normalize $\epsilon_0 = \mu_0 = 1$ and $\omega = c = 1$. Also, we set $m_e = 1$ and $e = -1$. From this it follows that $w_c = -B_0$ and $w_p^2 = N_e$. We consider the following two cases:

- case $N_e \neq$ const, no resonance;
- case $N_e \neq$ const, resonance.

For every fixed absorption rate ν, in the time domain we choose the boundary conditions of the form

$$\begin{aligned} \partial_t H|_{x=-L} &= -\partial_x E_y|_{x=-L} = G\sin(t),\ G \in \mathbb{R}, \\ \partial_t H|_{x=H} &= 0, \end{aligned} \tag{22}$$

and zero initial conditions, and in the frequency domain

$$\partial_x \hat{E}_y\Big|_{x=-L} = G,\ \partial_x \hat{E}_y\Big|_{x=H} = 0.$$

We compute the solution $\mathbf{E}^\nu(t)$ for large t in the time domain (the solution computed numerically at the time step n is denoted by $\mathbf{E}^\nu_n$), and the solution $\hat{\mathbf{E}}^\nu$ in the frequency domain. In the numerical experiments we check whether the following two quantities

$$\lim_{t\to+\infty} \mathbf{E}^\nu(t),\ \text{and}\ \Im\left(\hat{\mathbf{E}}^\nu \exp(it)\right)$$

are close as $\nu \to 0$ (provided that the first of these quantities exists).

In all the experiments in this section the CFL number was chosen as 0.5.

4.3.1. *No-Resonance Case*

We choose the parameters so that in the frequency domain, for the limiting amplitude problem, $\hat{E}^\nu_y$, $\nu = 0$, satisfies the Airy equation, c.f. also Remark 2.2. We set $\omega_c = 0$ (thus $\delta(x) = 0$), $\omega = 1$ (hence $\alpha(x) = 1 - N_e(x)$), choose the domain as $(-0.5, 10)$ and set the electron density $N_e(x) = 1 + x$. Importantly, $N_e(x) > 0$ on the whole interval. The boundary conditions in (22) are chosen as $G = Ai'(0.5)$.

First we set $\nu = 10^{-2}$. To demonstrate that the limiting amplitude principle indeed holds, we fix a point $x = x_c$ inside the domain and plot the dependence of the solution $E^\nu_y(x_c, t)$, $\Im\left(\hat{E}^\nu_y(x_c)\mathrm{e}^{it}\right)$ on time t for a range of $t \gg 1$ in Fig. 7. We compare this solution to the computed $\Im\left(\hat{E}^\nu_y \mathrm{e}^{it}\right)$, for fixed values of t. Both solutions appear to be in close agreement.

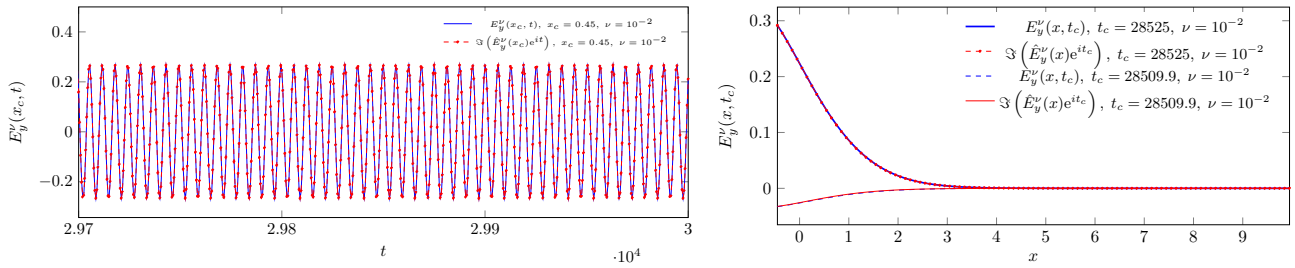

FIGURE 7. Dependence of the solution $E^\nu_y(x_c, t)$ on time for large times is demonstrated in the left figure. In the right figure we show the solution for $\nu = 10^{-2}$, for two fixed moment of times.

The computed L_2 error

$$\mathcal{E}_{x,y}(t) = \|\Im\left(\hat{E}^\nu_{x,y}\mathrm{e}^{it}\right) - E^\nu_{x,y}(t)\|_{L_2(-L;H)} \tag{23}$$

for $\nu = 10^{-2}$ did not exceed $1.1e-3$ for values of $t \in (28501, 30000)$. Fig. 8 (left) shows the solutions at a fixed point in space for $\nu = 1e-4$. As previously, we fix a point $x = x_c$ inside the domain and plot the dependence of the solution $E^\nu_y(x_c, t)$ on time t for a range of $t \gg 1$. The error (23) for $\nu = 10^{-4}$ at the time interval [228000.05, 240000.05] does not exceed 2.8e-4. One of our observations was that for smaller ν one requires more time steps to achieve the limiting amplitude solution. For $\nu = 10^{-4}$ we were not able to obtain the limiting amplitude solution for $t < 3 \cdot 10^4$, unlike in the case of $\nu = 10^{-2}$. For example, for $\nu = 10^{-6}$ we were not able to reach the limiting amplitude solution even on the time interval $t \le 1.92e6$, see Fig. 8 (right).

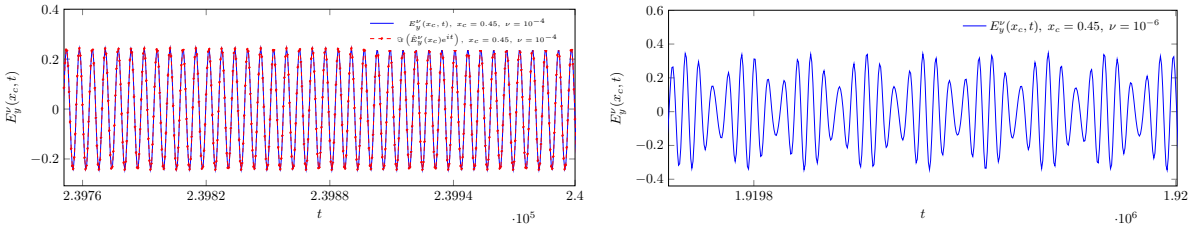

FIGURE 8. In the left figure we plot the dependence of the solution $E_y^\nu(x_c,t)$ on time t, with $\nu = 10^{-4}$ and $x_c = 0.45$. In the right figure we show the solution for $\nu = 10^{-6}$ at the same point x_c, for larger times. As we can see, for $\nu = 10^{-4}$ the limiting amplitude solution was reached for large t. For $\nu = 10^{-6}$ we were not able to obtain the limiting amplitude solution even for $t \approx 1.9e6$.

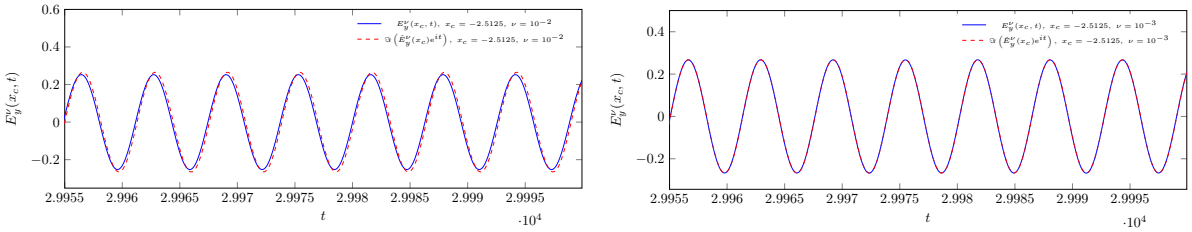

FIGURE 9. The figures demonstrate the dependence of the solutions $E_y^\nu(-2.5125,t)$ on time t for different values of ν.

4.3.2. *Resonance Case*

For the resonance case, we choose the parameters as in Table 2. Since $\alpha(x) = (1 - 2N_e(x))$, $\alpha(0) = 0$, and

Parameter	Value
L	5
H	19
ω_c	$\sqrt{0.5}$
$N_e(x)$	$\begin{cases} 0.25, & x < -0.5, \\ \frac{1+x}{2}, & x \geq -0.5, x \leq 9 \\ 5, & x > 9. \end{cases}$
G as in (22)	0.11

TABLE 2. Parameters for numerical simulations in Section 4.3.2

clearly, $\delta(0) \neq 0$. We compare the results for $\nu = 10^{-2}$, 10^{-3}, 10^{-4} in Fig. 9, 10, 11, 12, 13. The harmonic dependence of the solution on time is demonstrated by fixing x_c inside the domain and plotting $E_x^\nu(x_c,t)$ and $E_y^\nu(x_c,t)$ for a range of t.

Figures 11, 12, 13 show that in the case of the resonance the solution achieves the limiting amplitude solution, and both solutions are in close agreement (but in the points close to a point where the resonance occurs). These numerical results show that the staggered scheme resolves the resonance, similarly to the semi-lagrangian scheme described before. Like in the regular case, longer computations are needed to achieve the limiting amplitude solution for smaller ν.

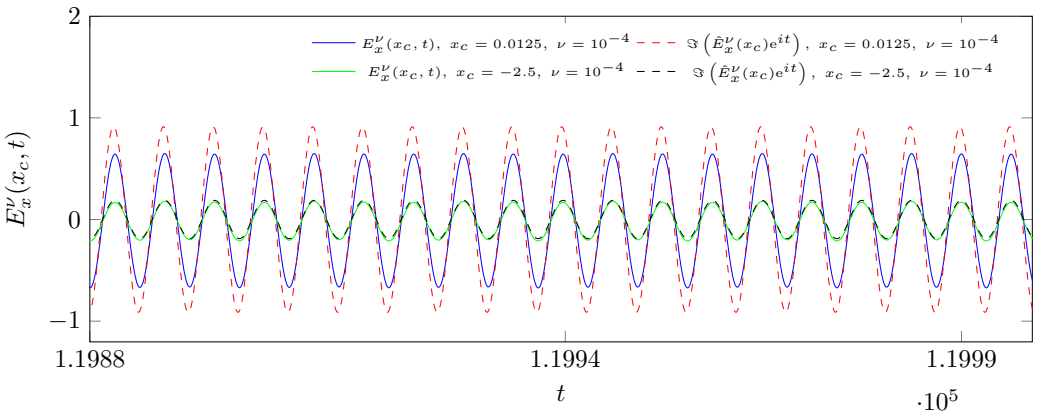

FIGURE 10. The plot shows the dependence of the solution $E_x^\nu(x_c,t),\ \nu=10^{-4}$ on time t for fixed $x_c=0.0125$ and for $x_c=-2.5$. We can see that the solutions computed in the time domain are in close agreement with the solution computed in the frequency domain at the point $x_c=-2.5$, however, differ at the point 0.0125 which is close to the $x=0$ where the resonance occurs.

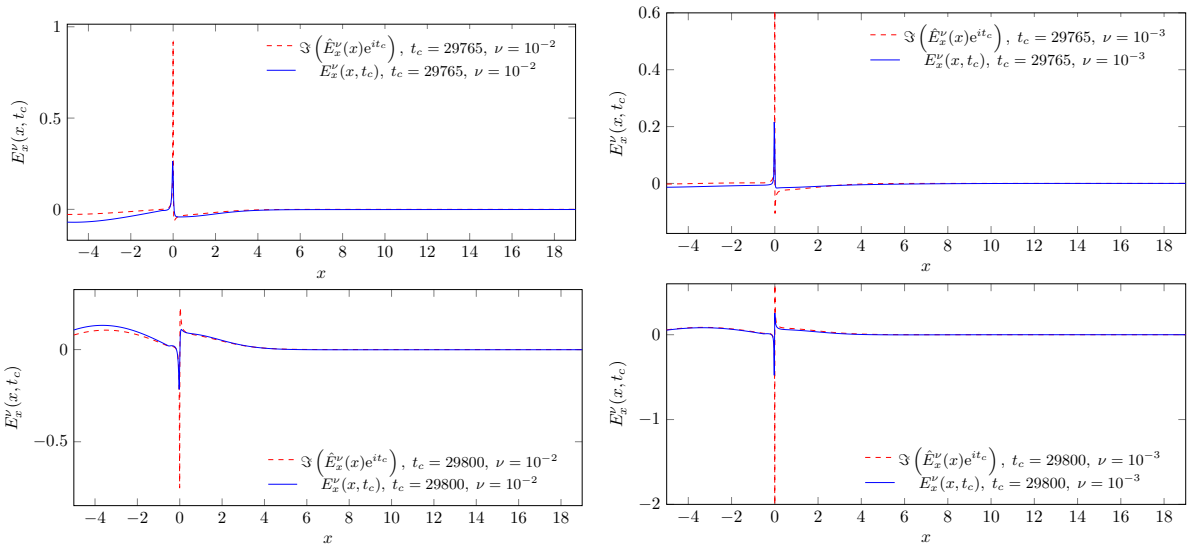

FIGURE 11. The figures demonstrate the dependence of the solutions $E_x^\nu(x,t)$ on x for fixed values of t.

5. Conclusions

In this work we considered the frequency- and the time-domain formulations of the X-mode Maxwell equations. In particular, we proved the well-posedness of the respective regularized (with the help of the absorption parameter ν) variational formulation, as well as studied the convergence of the finite element method for the problem with the resonance. The piecewise-constant FEM approximates the resonant solution rather well, at least for moderate values of ν, however, the discretization size should be chosen roughly proportional to $\nu^{\frac{7}{4}}$, in order to obtain an accurate discretization. Indeed, it would be interesting to look at the convergence of the

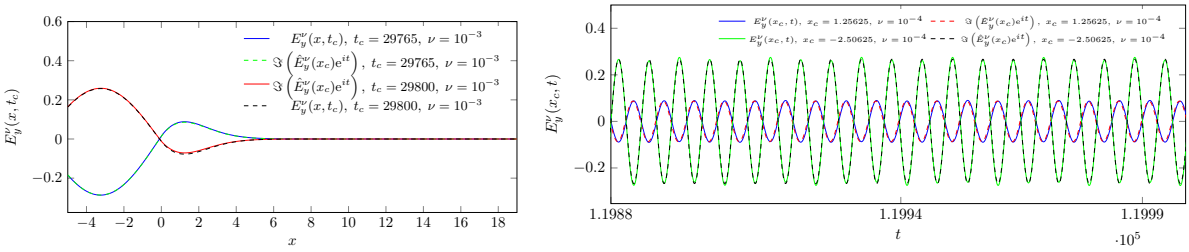

FIGURE 12. The left figure demonstrates the dependence of the solution $E_y^\nu(x,y)$ on x for fixed values of t. For a chosen value of ν the solutions computed in the time domain are in close agreement to the solutions computed in the frequency domain. This seem to be only partially true for the computed values $E_x^\nu(x,t)$ in this case (which may be caused by the discretization). The right figure shows the dependence of the solution $E_y^\nu(x,t)$ for $\nu = 10^{-4}$ on time for fixed $x = x_c$. We can see that the while the limiting amplitude principle holds true, the difference between the solutions computed in the time and frequency domain is not visible on this scale (c.f. Figure 13).

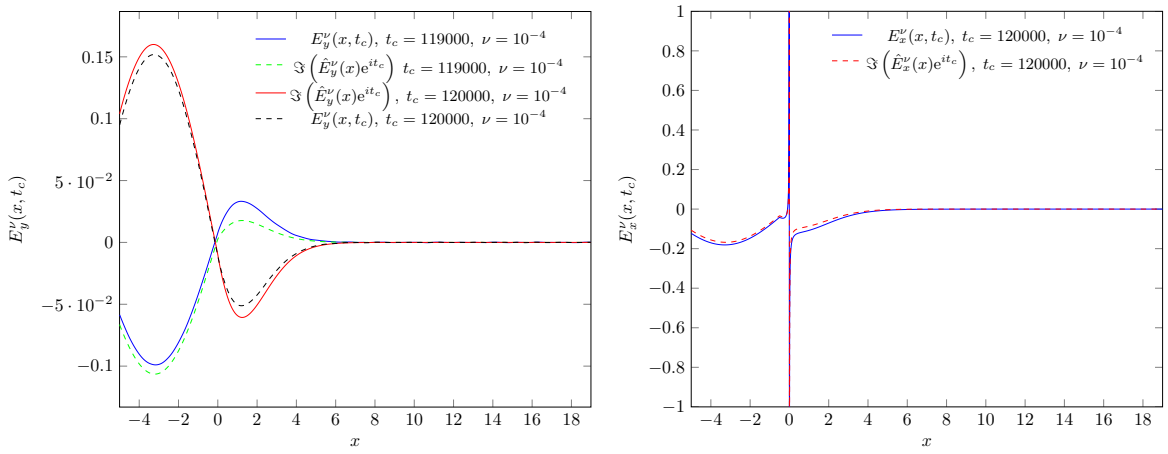

FIGURE 13. The figures demonstrate the dependence of the solutions $E_x^\nu(x,t)$ and $E_y^\nu(x,y)$ on x for fixed values of t. While the solution in the time-domain in the resonance point $x = 0$ has a smaller absolute value than that computed in the frequency domain (in the plot both solutions are truncated to axis limits), in other points the values are rather close.

adaptive finite elements for this kind of problems. Another unanswered question is the well-posedness of the discrete problem when the continuous problem is ill-posed. We have demonstrated by numerical means that while the condition number of the FEM matrix grows, the matrix remains always invertible, even for $\nu = 0$.

We proposed two different schemes for solving the time-dependent problem. Our numerical experiments demonstrate that both of them capture the singular behaviour of the solutions in the resonant case.

The other part of the experiments concerned the equivalence of the limiting absorption and limiting amplitude solutions. We have shown that for small ν and large times the solution computed in the time domain is close to the solution predicted by the limiting amplitude principle; as $\nu \to 0$, the solution oscillates harmonically as $t \to +\infty$, however, we were not able to compute the limiting amplitude solution for very small values of ν.

References

[1] Abramowitz M. and Stegun I. A., eds. (1972). Handbook of Mathematical Functions with Formulas, Graphs, and Mathematical Tables. New York: Dover Publications. Handbook of mathematical functions

[2] Brenner, S. C. and Scott, R. (2008). The mathematical theory of finite element methods (Vol. 15). Springer.

[3] Charles, F., Després, B., Merhenberg, M, Enhanced convergence estimates for semi-lagrangian schemes Application to the Vlasov-Poisson equation, SIAM J. Numer. Anal. 2013, 51(2), 840-863.

[4] Da Silva, F., Campos-Pinto, M., Després, B., and Heuraux, S. (2014). Stable coupling of the Yee scheme with a linear current model.

[5] S. Del Pino, B. Després, P. Havé, H. Jourdren, and P. F. Piserchia. 3D finite volume simulation of acoustic waves in the earth atmosphere. Comput. & Fluids, 38(4):765-777, 2009.

[6] Da Silva, F., Heuraux, S and Manso, M. (2006). Developments on reflectometry simulations for fusion plasmas: application to ITER position reflectometers. Journal of plasma physics, 72(06), 1205-1208.

[7] Da Silva, F., Heuraux, S., Gusakov, E. Z., and Popov, A. (2010). A Numerical Study of Forward-and Backscattering Signatures on Doppler-Reflectometry Signals. Plasma Science, IEEE Transactions on, 38(9), 2144-2149.

[8] Després, B., Imbert-Gérard, L. M. and Weder, R. (2014). Hybrid resonance of Maxwell's equations in slab geometry. Journal de Mathématiques Pures et Appliquées, 101(5), 623-659.

[9] Dumont, R. J., Phillips, C. K., and Smithe, D. N. (2005). Effects of non-Maxwellian species on ion cyclotron waves propagation and absorption in magnetically confined plasmas. Physics of Plasmas (1994-present), 12(4), 042508.

[10] Freidberg, J. P. (2007). Plasma physics and fusion energy. Cambridge university press.

[11] T. Hattori, T. (2014). Décomposition de domaine pour la simulation Full-Wave dans un plasma froid. Ph.D. Thesis, Université de Lorraine.

[12] Imbert-Gérard, L. M. (2013). Analyse mathématique et numérique de problèmes d'ondes apparaissant dans les plasmas magnétiques (Doctoral dissertation, Université Pierre et Marie Curie-Paris VI).

[13] Simon Labrunie, Pierre Bertrand, Jean-Rodolphe Roche, Aurore Back, Takashi Hattori, Electromagnetic wave propagation and absorption in magnetised plasmas: variational formulations and domain decomposition, Hal preprint 2014, https://hal.archives-ouvertes.fr/hal-01075137.

[14] Morawetz, C. S. (1962). The limiting amplitude principle. Communications on Pure and Applied Mathematics, 15(3), 349-361.

[15] Stix, T. H. (1992). Waves in plasmas. Springer.

[16] Xu, L., ans Yuan, N. (2006). FDTD formulations for scattering from 3-D anisotropic magnetized plasma objects. Antennas and Wireless Propagation Letters, IEEE, 5(1), 335-338.